Reliability improvement of the dredging perception system
A sensor fault-tolerant strategy

Wang, Bin; Zio, Enrico; Chen, Xiuhan; Zhu, Hanhua; Guo, Yunhua; Fan, Shidong

DOI
10.1016/j.ress.2024.110134

Publication date
2024

Document Version
Final published version

Published in
Reliability Engineering and System Safety

Citation (APA)
Wang, B., Zio, E., Chen, X., Zhu, H., Guo, Y., & Fan, S. (2024). Reliability improvement of the dredging perception system: A sensor fault-tolerant strategy. *Reliability Engineering and System Safety*, *247*, Article 110134. https://doi.org/10.1016/j.ress.2024.110134

Reliability Engineering and System Safety 247 (2024) 110134

Contents lists available at ScienceDirect

Reliability Engineering and System Safety

journal homepage: www.elsevier.com/locate/ress

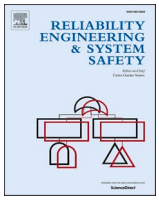

Reliability improvement of the dredging perception system: A sensor fault-tolerant strategy

Bin Wang [a,b,c,d], Enrico Zio [b,e], Xiuhan Chen [f], Hanhua Zhu [a,h], Yunhua Guo [a,h], Shidong Fan [c,d,g,*]

[a] School of Naval Architecture, Ocean and Energy Power Engineering, Wuhan University of Technology, Wuhan, China
[b] Energy Department, Politecnico di Milano, Milan, Italy
[c] State Key Laboratory of Maritime Technology and Safety, Wuhan University of Technology, Wuhan, China
[d] National Engineering Research Center for Water Transport Safety, Wuhan, China
[e] Mines Paris - PSL University, CRC, Sophia Antipolis, France
[f] Section Offshore & Dredging Engineering, Delft University of Technology, Delft, the Netherlands
[g] School of Transportation and Logistics Engineering, Wuhan University of Technology, Wuhan, China
[h] Key Laboratory of Marine Power Engineering & Technology, Ministry of Transport, PRC, Wuhan, China

ARTICLE INFO

Keywords:
Fault tolerant (FT)
Reliability
Sensor-fault detection, Isolation and accommodation (SFDIA)
Data fusion
Cutter suction dredger (CSD)
Dredging perception system

ABSTRACT

In the dredging industry, the automation and accuracy of the Dredging Perception System (DPS) are vital for operational efficiency and environmental safety. Current DPS implementations face challenges with sensor fault tolerance, leading to system unreliability and increased false alarm rates that can disrupt dredging operations. We propose a Hybrid Redundancy Sensor Fault Tolerance (HRSFT) strategy that integrates matching physical sensors (PS) with two distinct types of virtual sensors (VS) driven by multi-sensor association and time-series prediction models. The HRSFT employs a voting-cold storage strategy to address the false alarm issues commonly associated with single virtual sensor systems. Through experimental validation, the HRSFT strategy has demonstrated its capability to provide accurate replacement information during both single and multi-sensor failure scenarios, effectively managing abnormal sensor data and enhancing the operational reliability of the DPS. The implementation of the HRSFT strategy significantly improves the accuracy and stability of the DPS, suggesting a substantial advancement in sensor fault tolerance that could be applied to similar systems in various industries, leading to safer and more reliable operations.

1. Introduction

Dredging is essential for maintaining navigational channels, water quality and ensuring safe passage of ships. Over the years, the dredging industry has undergone significant changes, with AI technology playing a significant role in the automation of dredging systems. The DPS is a key component of an automated dredging system. The DPS uses sensors to detect the position of the dredger and the depth of the water, and this information is used to control the dredger's movement [1,2]. However, the DPS is vulnerable to faults that can result in loss of system's performance. Sensor faults, in particular, can cause significant damage to the dredger and environment. For instance, one of the environmental impacts related to dredging is increased suspended sediment concentration (SSC) levels, forming dredge plumes originating from spillage of dredged material. Concentration meters are effective in assessing plume dispersion. Therefore, it is critical to develop a sensor fault-tolerant design for the DPS to improve its reliability [3].

The issue, can be tackled by both Hardware Redundancy (HR) and Analytical Redundancy (AR) [4–8]. HR- based sensor fault detection, identification and accommodation is widely used in aerospace systems and self-driving vehicles [9–12]. However, there is a growing number of applications where cost, weight and size are critical design constraints. For these applications, AR-based sensor fault-tolerant methods are very attractive to increase reliability by intelligent systems. In 1971, Beard introduced the concept of fault detection filter, which marked the beginning of fault diagnosis technology based on AR [13]. The AR technology utilizes a mathematical model of the system to provide redundant information of sensor signals without increasing the number

* Corresponding author at: School of Transportation and Logistics Engineering, Wuhan University of Technology, Wuhan, China.
E-mail address: sdfan@whut.edu.cn (S. Fan).

https://doi.org/10.1016/j.ress.2024.110134
Received 24 May 2023; Received in revised form 5 March 2024; Accepted 4 April 2024
Available online 9 April 2024

of sensors; this allows improving the fault tolerance of the system and effectively overcome the limitations of HR. Hence, it is increasingly applied to the fault-tolerant design of sensors in flight control systems [14–16]. AR can be pursued mainly by two approaches (and their hybridization): Model-based (MB) and Data-based (DB) [17–20]. The MB approach is based on mathematical models derived from the physical laws governing the system dynamics and reproduces the system response in different working conditions [21]. The performances are heavily dependent on the available domain knowledge about the system to build accurate models of its behavior. The DB approach does not require detailed knowledge of the physics of the system, as it derives empirical models directly from historical data. This makes it attractive for equipment fault diagnosis and remaining life prediction [22–24]. Cartocci et al. [25] proposed a robust data-driven multiple sensor fault diagnosis approach for aircrafts. The proposed approach utilizes an optimization algorithm to select the optimal set of sensors for fault diagnosis, based on their redundancy and reliability. The approach is shown to be effective in diagnosing multiple faults with a high degree of accuracy. Darvishi et al. [26] proposed a SFDIA approach using a modular data-driven architecture. The approach uses a set of local fault detectors and estimators, which communicate with each other to ensure that the digital twin remains accurate and reliable. Another approach to SFDIA is to use deep learning for event identification and signal reconstruction in nuclear power plants with sensor faults [27]. The approach uses a convolutional neural network (CNN) to identify events and a long short-term memory (LSTM) network to reconstruct signals. Simulation results demonstrate the effectiveness of the proposed approach in identifying events and reconstructing signals in nuclear power plants with sensor faults. Fault detection strategies for vehicle sensors have also been proposed. Zou et al. [9] proposed a fault detection strategy for vehicle wheel angle sensors using a LSTM network and an improved sequential probability ratio test (SPRT). The approach uses the LSTM network to preprocess the sensor data and the SPRT to detect faults. Simulation results demonstrate the effectiveness of the proposed approach in detecting faults in vehicle wheel angle sensors. Clustering-based sensor fault detection and diagnosis is another approach to SFDIA. Luo et al. [28] proposed a clustering-based approach for detecting and diagnosing sensor faults in a chilled water system. The approach uses a clustering algorithm to group similar sensor measurements and identify outliers. Simulation results demonstrate the effectiveness of the proposed approach in detecting and diagnosing sensor faults in a chilled water system. Statistical-divergence-based techniques also show advantages in sensor fault diagnosis; in particular, approaches based on Kullback-Leibler divergence (KLD) have been shown effective for SFDIA [29]. Arslan Ahmed Amin et al. [30] delved into the integration of machine learning, deep learning, and transfer learning for fault diagnosis in Fault-Tolerant Control systems, highlighting the importance of these systems in safety-critical applications and providing a valuable resource for researchers in this domain.

In prior research work, the authors have addressed the issue of the high frequency of sensor failures during CSD construction, due to the challenging environment [31,32]. Missing or wrong sensor data can affect the success of the construction process. Then, we have proposed a slurry concentration soft-sensor model, by allocating other highly reliable sensors on the CSD and learning the construction data to predict the values of key parameters while the dredger is running. The proposed method was validated on a CSD construction case study, showing high prediction accuracy and low computational cost. Li et al. [33] proposed a digital twin-driven virtual sensor (DTDVS) approach to ensure the safe operation of Trailing Suction Hopper Dredger (TSHD). By analyzing the residual between the values of the physical and virtual sensors, it is possible to detect fault conditions. The DTDVS approach improves TSHD's time utilization and provides an essential guarantee for construction safety.

However, the above methods have difficulties in dealing with multi-sensor failures. A virtual sensor constructed by only one data-driven model is not able to maintain stability of the whole perception system when dealing with the effects of multi-sensor failures, thus, compromising the automation and unmanned dredging operations.

The purpose of this work is to improve the reliability of the DPS by a sensor fault-tolerant strategy. An HRSFT system based on two data-driven models is proposed to detect and identify failures of sensors, and produce replacement information of the failed sensors using weighted least squares. The main contributions are:

- Innovative Fault-Tolerance Design for Dredging Operations: For the first time in the field of dredging, we propose a sensor fault-tolerance design that addresses the unique environmental and operational requirements of dredging vessels. This approach significantly enhances the reliability of dredging perception systems during continuous operations.
- Hybrid Redundancy in Sensor Systems: A hybrid redundancy design for sensor systems is developed, which is a novel approach in the field. Unlike traditional methods, this design combines various redundancy techniques to ensure higher system reliability and fault tolerance, especially in challenging operational conditions.
- Effective Multi-Sensor Fault Detection Method: The proposed method introduces a new hybrid redundancy approach for sensor fault tolerance. This method is more effective in identifying and handling sensor faults, especially in scenarios with simultaneous failures in multiple sensors, a common challenge in dredging operations.
- Enhanced Sensor System Performance through Information Fusion: Our research presents a hybrid redundancy sensor information fusion method. This method improves the measurement accuracy during sensor degradation phases and extends the service life of sensors. It represents a significant advancement in sensor technology, particularly in the demanding context of dredging operations.

The rest of this paper is organized as follows. Section 2 briefly provides an overview of the DPS and the dredging technology. Section 3 describes the proposed sensor fault-tolerant operation strategy and system design. Then, the reliability estimation and improvement of DPS is introduced in Section 4. Section 5 highlights and compares the performance of the hybrid-redundancy sensor strategy for different sensor faults. Some conclusions are eventually drawn in Section 5.

2. Problem description

In the context of dredging operations, the reliability and accuracy of the DPS are crucial. The DPS, equipped with various sensors, plays a pivotal role in navigation and operational efficiency. However, the system encounters significant challenges:

- One of the primary challenges in DPS is managing simultaneous failures of multiple sensors. Such scenarios are increasingly common in the complex and demanding environments of dredging operations. Traditional sensor systems, including those based on HR and AR, often fall short in these situations. This inadequacy can lead to severe disruptions in operations and compromise the safety of unmanned dredging systems. The need for a robust solution that can handle such complexities is therefore paramount.
- Another issue is the inevitable degradation of sensor system performance over time. Traditional systems lack mechanisms to enhance or even maintain performance throughout their operational lifespan. This gradual decrease in sensor efficiency results in reduced accuracy and reliability, which are critical for the safe and effective functioning of dredging operations.

Given these challenges, our study introduces a novel approach – a HRSFT system. This system, utilizing dual data-driven models, aims to efficiently detect and manage sensor failures, as well as improve sensor

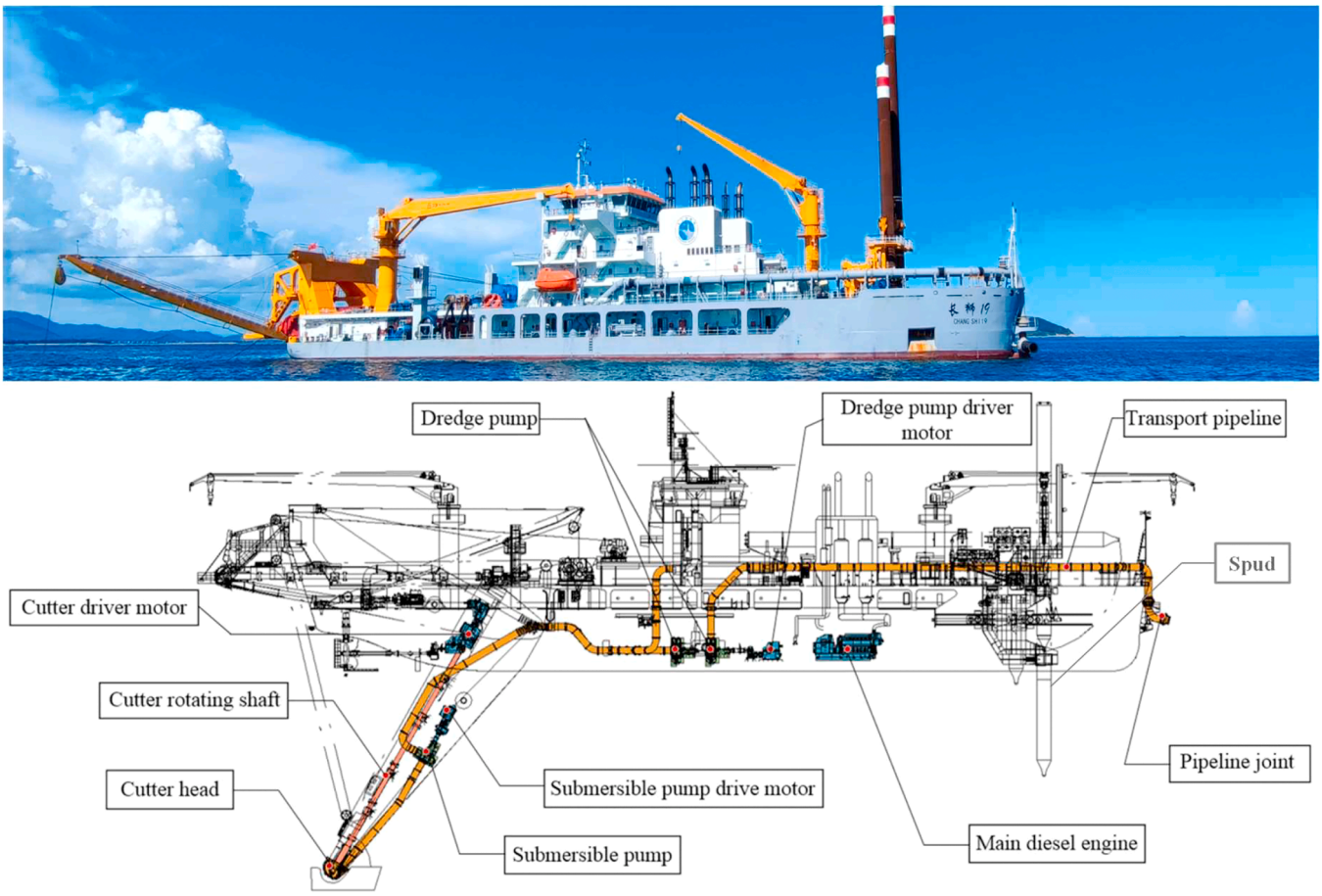

Fig. 1. "CHANGSHI 19" cutter suction dredger.

performance over time through innovative information fusion techniques. The proposed system is tailored to meet the unique environmental and operational demands of dredging vessels, enhancing the overall reliability of the DPS. These issues highlight the need for a more advanced and adaptive sensor fault-tolerance strategy in dredging operations, to ensure continuous performance and safety in various operating conditions. Our approach seeks to address these challenges, paving the way for more reliable and efficient automated dredging operations.

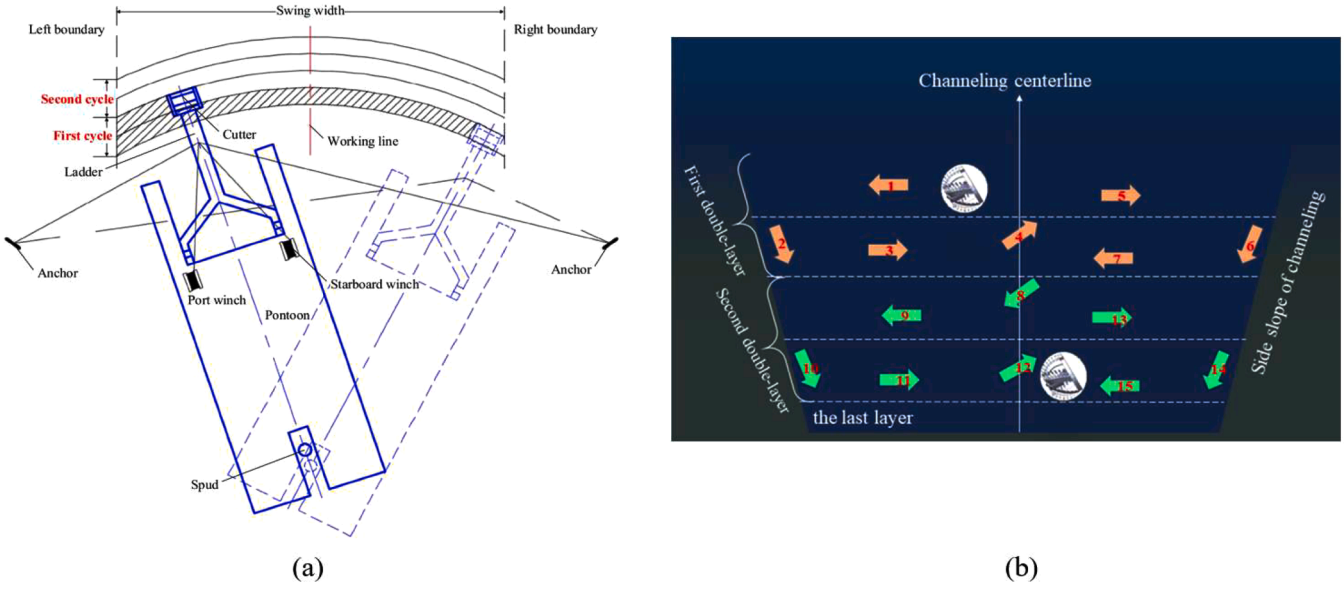

Fig. 2. The dredging process of a cutter suction dredger.

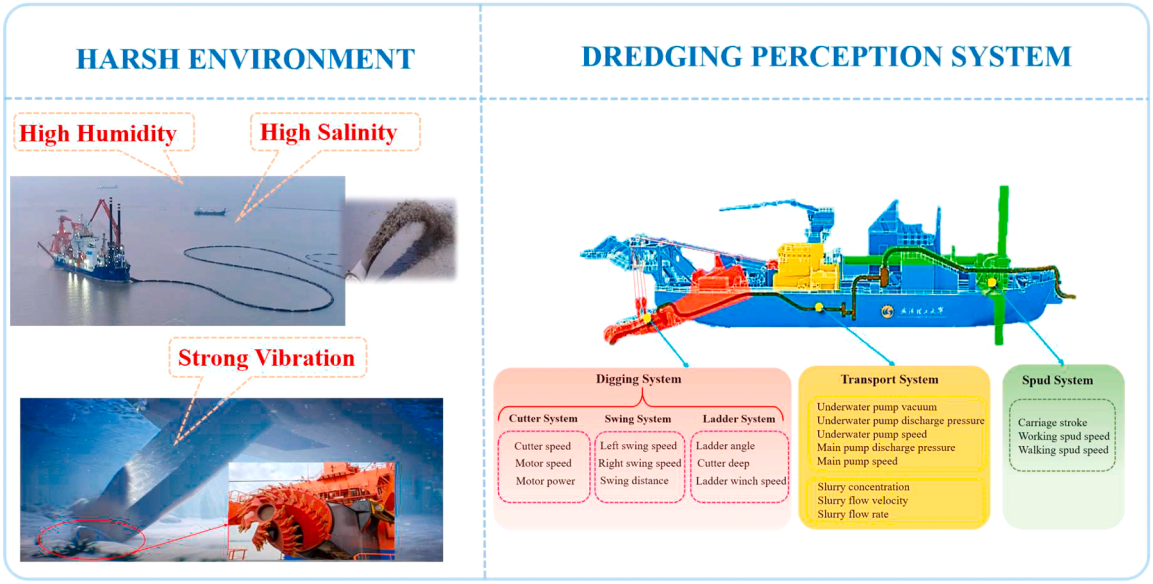

Fig. 3. The DPS and dredging environment of a cutter suction dredger.

3. Overview of the dredging perception system

3.1. Dredging technology and process

For illustration, we consider the DPS of the "CHANGSHI 19″ CSD shown in Fig. 1. In general, at the bow of the dredger, there are two heavy-duty positioning steel spuds, one of which is driven into the submerged ground to maintain the dredger's position during construction operations. The ladder is connected to the hull through two ladder-trunnion supports, and the winch is used to raise or lower it. Typically, one or two in-board pumps are installed in the slurry pump compartment, and some dredgers may have submerged slurry pumps on the cutter ladder, which are typically located near the mud suction port. The cutter is installed at the suction port of the slurry suction pipe and is usually driven by the cutter motor installed at the upper end of the cutter ladder or directly by the motor of the submerged pump (Fig. 1).

The CSD is a special type of ship used for channel excavation, port maintenance and island reclamation, whose dredging system includes cutter cutting system, slurry conveying system, swing control system and spuds system. In general, the CSD mainly relies on manual operation by operators. Specifically, the operators need to monitor the relevant operating parameters of the dredger in real-time. The construction operation of a CSD involves controlling two side anchor cables, one retracted and one released, to make the dredger fan-shaped swing dredging around the positioning steel spud. The cutter cutting system of the CSD consists of several components, including a front-end device, cutter, cutter drive shaft, mud-absorbing baffle, mud-absorbing port, and underwater pipeline. This system is designed to cut and crush mud, sand, or rock underwater, forming a mixture that is then connected to the suction and discharge pipeline through the suction port. The swing process is shown in Fig. 2(a). The working spud is installed on the spud carriage and can be moved back and forth in the dredger bow, whereas the walking spud is installed in an eccentric position at the bow of the dredger to play the role of pile replacement and auxiliary positioning. Typically, the CSD takes a steel spud or three cable guides as the swing center, driving the dredger to swing laterally through the left and right side anchors for dredging operation. The hydraulic cylinder pushes the carriage to travel a distance to complete a feed when cutter swinging to the dredging edge line. Then, the cutter head swings back to the other side of the dredging line to complete the next feed. When the carriage travels the whole distance, the CSD moves across the dredge to the other side of the dredging line to complete the next feed. Once the dredger is fully traveled, it moves across to the centerline of the dredging trench, lifts the bridge, tightens the traverse cables at both ends, puts the walking spud down, and raises the working spud simultaneously. It then presses the working spud into the soil and raises the walking spud. The carriage completes one running stroke and starts the second running stroke. Fig. 2(b) illustrates the diagram of dredging different geological materials layers.

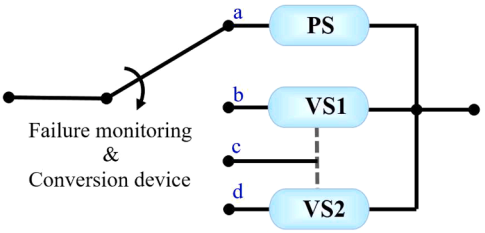

Fig. 4. Diagram of the hybrid redundancy sensor structure.

3.2. DPS and dredging environment

As the intelligence level of dredgers continues to improve, the number of sensors installed on dredgers is creasing. In the light of practice, there are now more than 200 monitoring sensors, and that number may continue to grow. However, there are currently no standardized norms and regulations regarding the use of sensors for key operating equipment on dredgers within the dredging industry. As a result, the sensors installed on each dredger's key operating equipment often operate under an excessive workload. Coupled with the harsh operating conditions of the dredging site, which includes a high salt, high humidity, and strong vibration environment, these sensors are susceptible to performance degradation and failure throughout the year. Fig. 3 displays the dredging perception system of a CSD.

In this setting of the perception system poses a significant safety hazard and has become a hindrance to the development of intelligent dredging. It is, therefore, crucial to take effective measures to ensure the reliability of the perception system for key equipment during continuous dredging operations.

Algorithm 1
HRSFT Operation Strategy Algorithm.

Input: Training set $D=\{(x_1,y_1),(x_2,y_2),\cdots,(x_m,y_m)\}$;
Virtual sensor *1* (***VS1***) ; Virtual sensor *2* (***VS2***); Detection threshold δ

Output: Physical Sensor (***PS***); Fusion Sensor (***FS***)

Process:

for $t=1,2,...,T$ **do**
  $\gamma_t = VS1_t(D)$
  $\chi_t = VS2_t(D)$
end
for $i=1,2,...,m$ **do**
  if $alarm \leftarrow (\gamma_i-\delta)<0 \cap (\chi_i-\delta)<0$
    for $k=1,2,...,n$ **do**
      $\alpha_k,\beta_k \leftarrow$ *weighted least squares*
      $FS \leftarrow \alpha_k\gamma_k+\beta_k\chi_k$
    end
  else if *self dection* $\leftarrow (\gamma_i-\delta)(\chi_i-\delta)<0$
    $PS \leftarrow PS$
  else *normal* $\leftarrow$ *other*
    $PS \leftarrow PS$
  end
end procedure

Algorithm 2
Stacking Generalization Algorithm.

Inputs: Training sets $D=\{(x_1,y_1),(x_2,y_2),\cdots,(x_m,y_m)\}$
Base model $\Im_1,\Im_2,\cdots,\Im_T$
Meta-model $\Im$

Outputs: $H(x)=h'(h_1(x),h_2(x),...,h_T(x))$

Process:

for $t=1,2,...,T$ **do**
  $h_t=\Im_t(D)$
end for
$D'=\varnothing$
for $i=1,2,...,m$ **do**
  for $t=1,2,...,T$ **do**
    $z_{it}=h_t(x_i)$
  end for
  $D'=D'\cup((z_{i1},z_{i2},...,z_{iT}),y_i)$
end for
$h'=\Im(D')$

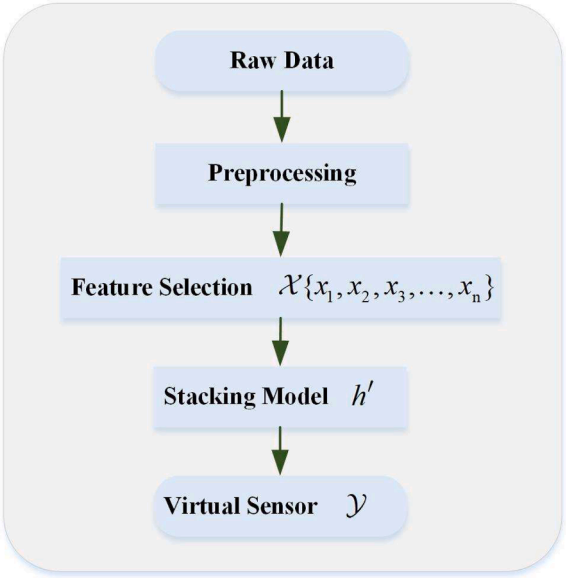

Fig. 5. The diagram of virtual sensor 1.

4. Sensor fault-tolerant operation strategy and system design

4.1. Hybrid redundancy sensor design

It is essential to design multiple mechanisms, ideally more than two, to enable the system to retain functionality even in the event that one of them fails, in order to improve the reliability of systems and ensure the completion of work. To this end, redundant systems like active, warm, and standby redundancies are generally employed [34,35].

This study proposes a "voting-cold storage" structure that combines the principles of virtual and physical sensors, as shown in Fig. 4. This structure is designed to enhance the dependability of the sensing unit and optimize the autonomous functioning of the system. In particular, the sensor fault detection system is configured so that a normal PS triggers the connection of interface **a**; whereas, when virtual sensor VS1 is identified as normal and VS2 as faulty, the connection is established through interface **b**. Conversely, when VS1 is faulty and VS2 is normal, interface **d** comes into operation. Moreover, when the physical sensor malfunctions, the system automatically activates interface **c**, which makes the fusion information from the two virtual sensors (Fig. 4).

In summary, the proposed structure presents a dependable and robust redundancy solution for complex systems. By combining virtual and physical sensors, it safeguards the reliability of the sensing unit, ensuring uninterrupted monitoring system performance, and maintaining the independence of its operation. The functional activation process is elaborated in Algorithm 1 and more details are introduced in the next section.

4.2. Virtual sensors

4.2.1. Virtual sensor 1 (VS1)

In this section, we explore the internal relationships between various sensing data from equipment by first using the maximal information coefficient approach. A multi-sensor association model is, then, developed using machine learning models like lasso, elastic net, gradient-boosting decision tree, extreme gradient boosting, and light gradient boosting machine. Finally, we combine the aforementioned models into VS1, a multi-sensor regression prediction model, using a stacking generalization method (refer to Algorithm 2 below).

Importantly, as the amount of available data for learning increases, the performance of the VS1 improves; therefore, the model has strong potential for increasing capability. Fig. 9 illustrates the process [32] (Fig. 5).

4.2.2. Virtual sensor 2 (VS2)

Based on the association information and a priori knowledge of each unit in the DPS, we have developed a time-series prediction method for sensing values using the CNN-LSTM Encode-Decode technique [36]. Our approach involves continuous analysis of the dredger construction process while taking into account the continuity and temporal characteristics of the time-series data from each sensing unit. We utilize the time-series self-movement time-window method to establish a virtual sensor for each sensing unit based on time series prediction. The diagram is presented in Fig. 6, as shown below.

4.3. Sensor anomaly detection based on hybrid redundancy

We coordinate the reconstructed virtual sensors and physical sensor to create a voting evaluation system using the residual configuration technique and voting monitoring method. Using the data-driven fault self-diagnosis method, we can successfully distinguish among sensor faults by calculating the structural residual values of the two virtual sensors separately.

The basic logic of sensor fault detection and isolation is illustrated in Fig. 7. The sensor is deemed faulty if both residual values concurrently exceed the threshold, in which case the system outputs the reconstructed signal created by fusing the weighted least squares estimates from the two virtual sensors. If the two residual values are below the threshold at the same time, the sensor is deemed to be normal, and the system outputs the physical sensor signal. In all other cases, the virtual sensor model with residual values above the threshold is asked to recalculate, but the system still outputs the physical sensor signal. To effectively distinguish between two similar signals of transient sensor overload and permanent failure, we have incorporated a finite state machine delayed link method [37]. This approach ensures that the residual signal must persist for a specified duration as determined by a counter loop, before it

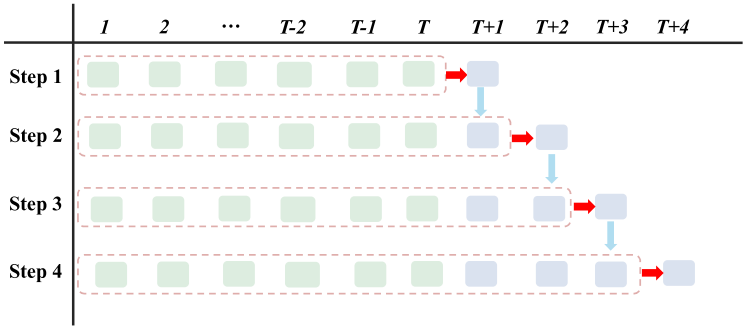

Fig. 6. The diagram of virtual sensor 2.

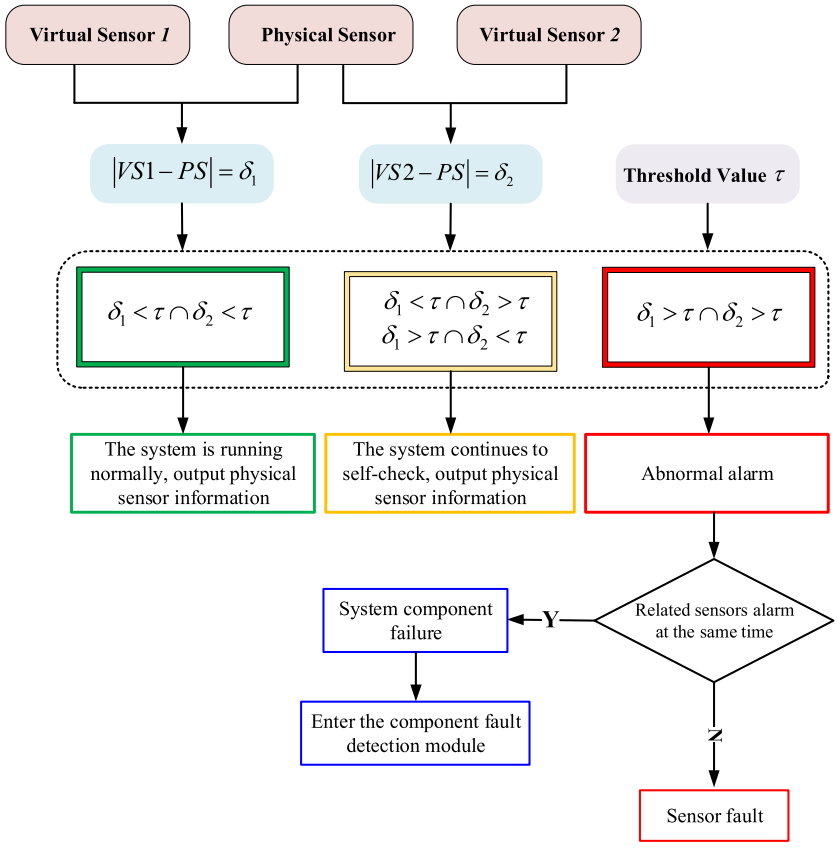

Fig. 7. The logic of sensor fault detection and isolation.

can be marked as a genuine sensor failure, thus meeting the needs of dredging operations (Fig. 7).

4.4. Information fusion output by virtual sensors

The reliability of sensing elements decreases with continuous use, resulting in reduced measurement accuracy and even malfunction. However, with increasing data, virtual sensors can become more accurate, thus improving the reliability of the perception system. Therefore, we fuse two virtual sensors to improve the accuracy of information and ultimately enhance the operational reliability of the perception system.

To simplify the calculation, we need to make some assumptions.

Assumption 1. The fusion method is measurement fusion, that is, the measurement of the sensor is directly sent to the fusion center for fusion processing, and the obtained state estimation is a global estimation.

Assumption 2. In the system, the sensor values for the same target are obtained at the same time, namely, time-synchronized measurements.

Here, $\hat{x}^1_{k|k}$, $P^1_{k|k}$and $\hat{x}^2_{k|k}$, $P^2_{k|k}$ represent the estimation of the target state x_k and its error covariance, respectively. $P^{1,2}_{k|k}$ represents the error cross-covariance between $\hat{x}^1_{k|k}$and $\hat{x}^2_{k|k}$. In general, the sensor measurement value as shown in Eq. (1).

$$\hat{x}^i_{k|k} = x_k + \mu^i_k \tag{1}$$

where $\mu^i_k$is the system or process noise, generally assumed to be a Gaussian random variable with 0 mean and known covariance, i.e., $\mu_k : \sim N(0, P^i_{k|k})$.

Hence, the measurement z_k of the target state x_k is obtained from the fusion sensors measurements x_1 and x_2 by Eq. (2).

$$z_k = Hx_k + \nu_k \tag{2}$$

where $z_k = [\hat{x}^1_{k|k}, \hat{x}^1_{k|k}]^T$, H is the measurement matrix, $H = [I \quad I]^T$, I is the identity matrix, $\nu_k$is the measurement noise, $\nu_k = [\nu^1_k, \nu^2_k]^T$ generally assumed to be a Gaussian random variable with 0 mean and known covariance, i.e., $\nu_k :\sim N(0, R_{k|k})$.

Moreover,

$$R_{k|k} = \begin{bmatrix} P^1_{k|k} & P^{1,2}_{k|k} \\ P^{2,1}_{k|k} & P^2_{k|k} \end{bmatrix} \tag{3}$$

duo to the symmetry of the covariance matrix, $P^{1,2}_{k|k} = P^{2,1}_{k|k}$.

The fusion estimation of the target state $\hat{x}_k$ can be obtained according to the weighted least squares estimation.

$$\hat{x}_k = \left[H^T R^{-1}_{k|k} H\right]^{-1} H^T R^{-1}_{k|k} z_k \tag{4}$$

The covariance of its estimation error is

$$P_{k|k} = \left[H^T R^{-1}_{k|k} H\right]^{-1} \tag{5}$$

e.g.

$$\hat{x}_k = \left[\begin{bmatrix} I & I \end{bmatrix} \begin{bmatrix} P^1_{k|k} & P^{1,2}_{k|k} \\ P^{2,1}_{k|k} & P^2_{k|k} \end{bmatrix}^{-1} \begin{bmatrix} I \\ I \end{bmatrix}\right]^{-1} \begin{bmatrix} I & I \end{bmatrix} \begin{bmatrix} P^1_{k|k} & P^{1,2}_{k|k} \\ P^{2,1}_{k|k} & P^2_{k|k} \end{bmatrix}^{-1} \begin{bmatrix} \hat{x}^1_{k|k} \\ \hat{x}^2_{k|k} \end{bmatrix} \tag{6}$$

$$P^{1,2}_{k|k} = \left[{P^1_{k|k}}^{-1} + {P^2_{k|k}}^{-1}\right]^{-1} \tag{7}$$

From Eq. (7), we can get $P^{1,2}_{k|k} < P^1_{k|k}$ and $P^{1,2}_{k|k} < P^2_{k|k}$, which shows that

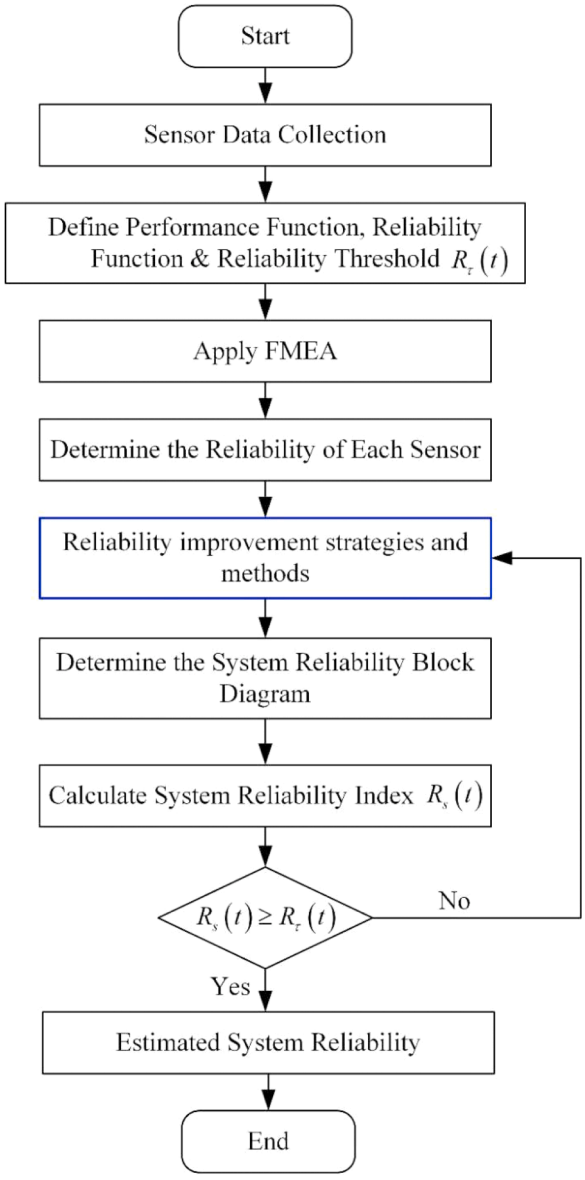

Fig. 8. The flow diagram of reliability estimation.

the error covariance of the fused information is smaller, i.e., the accuracy is higher.

5. Reliability estimation and improvement

To succinctly illustrate our process for assessing system reliability, we have presented a flowchart of the reliability estimation methodology in Fig. 8. It starts with the collection of sensor data, a crucial initial step to gather the necessary inputs for reliability analysis. Following this, the performance function, reliability function, and reliability threshold $R_r(t)$ are defined, setting the criteria for system evaluation. Next, Failure Mode and Effects Analysis (FMEA) is applied, a methodical approach to identify potential failure modes and assess their impact on the system. The reliability of each individual sensor is then determined, which forms the basis for understanding the system's overall reliability. Should any sensor's reliability not meet the set threshold, reliability improvement strategies and methods are implemented. This is an iterative process, indicating that if improvements are needed, the process may revisit previous steps. Once sensors meet the reliability criteria, the system reliability block diagram is determined. This diagrammatic representation helps to visualize the system's reliability structure and interdependencies. Subsequently, the system reliability index is calculated, representing a quantified measure of the system's reliability over time. A decision point follows where the system reliability index is compared against the predefined threshold. If the index is not satisfactory, the process loops back to the improvement strategies. If the index is satisfactory, the process concludes with an estimation of the system's reliability, indicating that the system is reliable enough for its intended function. The process ends here, signifying the completion of the reliability estimation (Fig. 8).

5.1. FMEA for sensor fault

In order to ensure the integrity of verification and simplify the workload, we use FMEA to select the most representative failure parameters for the safety and efficient operation DPS [38]. Severity(S), Occurrence (O), Detection (D) and Risk Priority Number (RPN) are indicators for FMEA [39], which process is presented in appendix (Fig. 9).

5.2. Operational reliability estimation

In the non-working redundancy system, also known as, a bypass system, only one of the n units is operating, and others are in reserve. When the working unit fails, it is connected to another unit to work through the failure monitoring and conversion device.

Assumption 3. the failure detection and switching are ideal, and which reliability both are 1.

When all units are the same and their lifetime distribution obeys the exponential distribution, the system reliability function is Eq. (8). Here, its distribution function obeys the Poisson distribution. Where n is the number of units that make up the system, λ is the unit failure rate.

$$R_s(t) = e^{-\lambda t}\left[1+\lambda t+\frac{(\lambda t)^2}{2!}+\cdots+\frac{(\lambda t)^{n-1}}{(n-1)!}\right] = e^{-\lambda t}\sum_{i=0}^{n-1}\frac{(\lambda t)^i}{i!} \tag{8}$$

When the bypass system consists of two different elements A1 ($R_1 = e^{-\lambda_1 t}$) and A2 ($R_2 = e^{-\lambda_2 t}$), one of which is in the operating state (A1) and the other in reserve (A2). The system work normally within time T, there are only two possibilities: one is that A1 has been working normally unit time T; the other is that A1 occurs a failure within time T, while A2 continues operation. Hence, its reliability mathematical model is:

$$R_s(t) = e^{-\lambda_1 t} + \frac{\lambda_1}{\lambda_1-\lambda_2}\left(e^{-\lambda_2 t}-e^{-\lambda_1 t}\right) \tag{9}$$

In the working redundancy system, when the pure parallel system is composed of n parallel elements of equal reliability, the system reliability is Eq. (10). Where $R_s$is the system reliability, $R$is the reliability of a single element.

$$R_s = 1-(1-R)^n \tag{10}$$

In the k-out-of-n system, assuming the n elements are all the same, then, the system reliability is Eq. (11). Where n is the number of units that make up the system, and k is the minimum number of units necessary for the system to function properly.

$$R_s = \sum_{i=0}^{n-k} C_n^i R^{n-i}(1-R)^i \tag{11}$$

When the reliability of each unit is the same, the reliability model of the redundant system with the series-parallel structure is shown in Eq. (12).

$$R_{sp} = 1-[1-R^n]^m \tag{12}$$

The reliability model of the parallel-series redundant system is:

$$R_{ps} = [1-(1-R)^m]^n \tag{13}$$

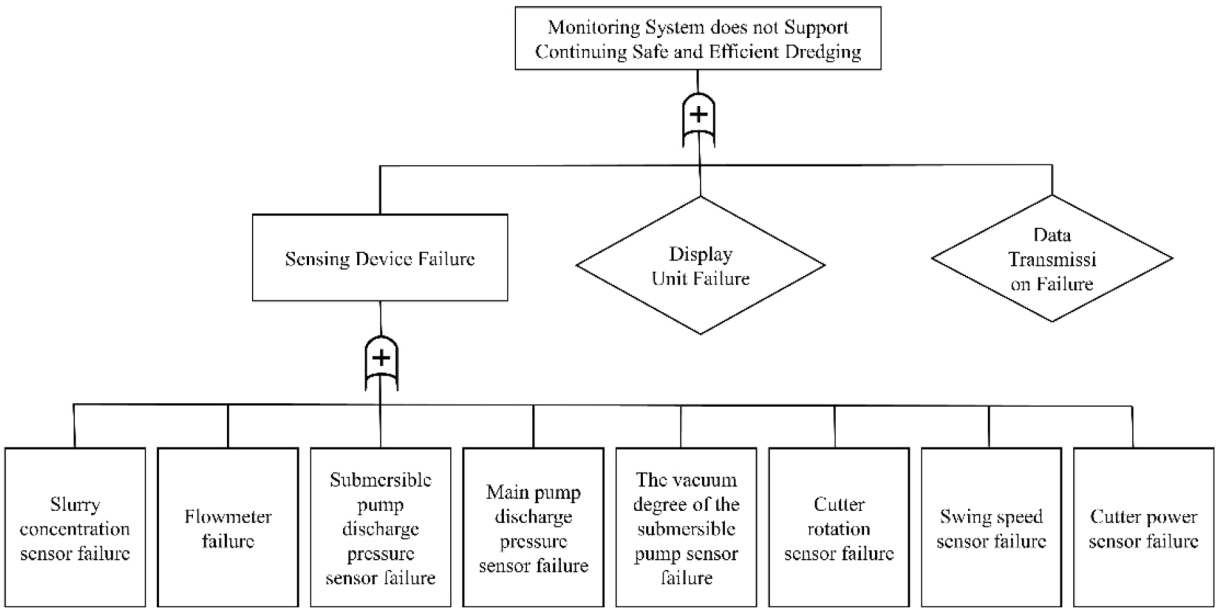

Fig. 9. The failure block diagram of the dredging operation sensing system.

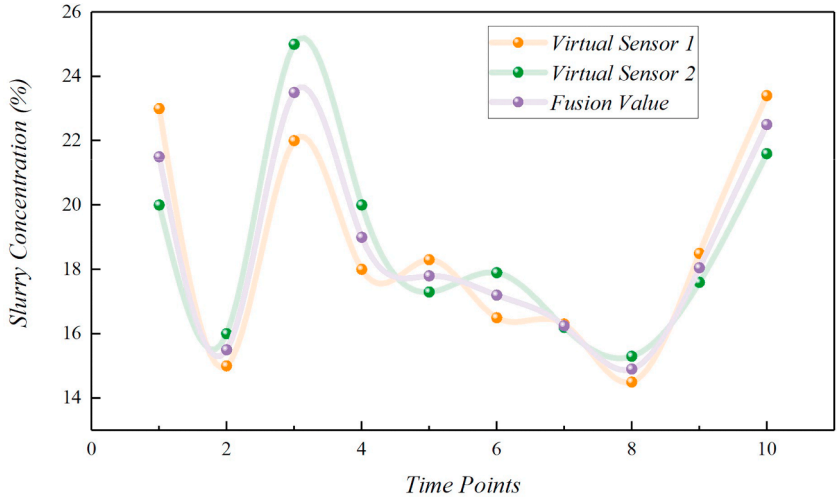

Fig. 10. Comparison of the fusion performance .

In the task mode of safe and efficient construction, the above eight parameters can be regarded as a simple series system, where the failure of any parameter will case the task to fail. From Fig. 8, the system reliability is:

$$R_S = R_{Device} \cdot R_{\text{Display}} \cdot R_{Trans} = \prod_{i=1}^{8} R_i \cdot R_{\text{Display}} \cdot R_{Trans} \tag{14}$$

where, R_{Device} is the reliability of DPS, R_{Display} is the reliability of sensing unit, R_{Trans} is the reliability of transmission system. $R_1 \cdots R_8$ are reliability of slurry concentration meter, reliability of flowmeter, reliability of discharge pressure gauge of underwater pump, reliability of discharge pressure gauge of main mud pump, reliability of pressure gauge of vacuum degree of underwater pump, reliability of cutter rotation measurement, reliability of swing speed measurement and cutter power measurement reliability, respectively.

In the safe and efficient mission mode, the Eq. (14) shows that the reliability of the DPS will becomes 0 (i.e., $R_s = 0$), when the slurry concentration meter fails during the working(i.e., $R_1 = 0$).

5.3. *Reliability improvement by redundancy information fusion*

Based on the assumption that the calculation error covariance of VS1 is 0.05, and VS2 is 0.01, the fused concentration value has an error covariance of 0.0083, as calculated using Eq. (7). This demonstrates that the weighted least squares optimal estimate is significantly better than using VS1 and VS2 alone. Therefore, by fusing data from multiple sources, we can achieve more accurate and reliable estimates, ultimately improving the operational reliability of slurry concentration and enhancing the reliability of the dredging operation sensing system. This approach can lead to safer and more efficient dredging operations (Fig. 10).

Likewise, we assume that the reliability of all units are 1 in Eq. (14), except the slurry concentration. Hence, the operational system reliability is $\widehat{R}_s = \widehat{R}_1 \times 1 \times \cdots \times 1$ at this time, because$\widehat{R}_1 > R_1$, so $\widehat{R}_s > R_s$. In the same way, other sensors also can be fused, and finally improving the reliability of the DPS. Obviously, as can be seen from Fig. 10, the

Table 1
Features selection.

Virtual Sensor 1	Correlation Features
Slurry Concentration	Slurry Flow
	Velocity of Flow
	Dredge Pump Rotational Speed
	Cutter Power
	Cutter Rotational Speed
	Dredging Depth
	Ladder Angle
	Vacuum of Submersible Pump
	Discharge Pressure of the Dredge pump

Table 2
Evaluation of virtual sensor models.

Models	*Indexes*		
	R^2	RMSE	MAE
Virtual Sensor 1	0.9689	1.3677	1.0141
Virtual Sensor 2	0.9421	1.8414	1.3016

fusion values are in the middle of the VS1 and VS2 in all the experiment data.

6. Results

The experimental and validation was performed considering a DPS data of the "CHANGSHI 19″ CSD. The experiment data consists of a total of 237 dimensions and 29,161 groups. Among these groups, 100 time-continuous groups are selected as the experiment data. Subsequently, the remaining data was split into training set with 80 % of the data and a test set with 20 % of the data according to the timeline.

We first considered single sensor faults of 100 time continuous groups, then double faults and multiple faults of the same period. Failure of a sensor could manifest in several ways. The most common fault models are bias, drift, freezing and random fault. In this paper, without loss of generality, we considered bias and drift faults to represent hard and soft failures, respectively. We assume the additive fault happens in $N + M$ consecutive samples when sensor output drifts up to the bias level ε with N time instants.

$$S(n) = \begin{cases} r(n) + \sigma(n) + \varepsilon(n - m + 1)/N, & 0 \le n - m < N \\ r(n) + \sigma(n) + \varepsilon, & N \le n - m < N + M \\ r(n) + \sigma(n), & else \end{cases} \tag{15}$$

Where $r(n)$ is the ideal measurement of the sensor and m is the starting time instant of the fault, while $\sigma(n)$ denotes the measurement noise. Sensor measurement in the experiment is including measurement noise (i.e. they provide $r(n) + \sigma(n)$). M is the number of consecutive samples that the drift fault remains at the saturated bias levelε.

To streamline our analysis, we focused on investigating sensor failures in the context of slurry concentration measurements. In Section 4.1, we identified the slurry concentration as the primary experimental object. To further our investigation, we selected dual sensor failure experiments involving the slurry concentration and the vacuum of the underwater pump. Additionally, we conducted multiple sensor failure experiments using the slurry concentration, the vacuum of the underwater pump, and the discharge pressure of the main pump. The bias errors ε for slurry concentration, vacuum of the underwater pump, and discharge pressure of the main pump were 10%, 0.1 *bar*, and 3 *bar*, respectively. Furthermore, we used the values of $m = 80$, $N = 90$, and $M = 10$ in Eq. (15).

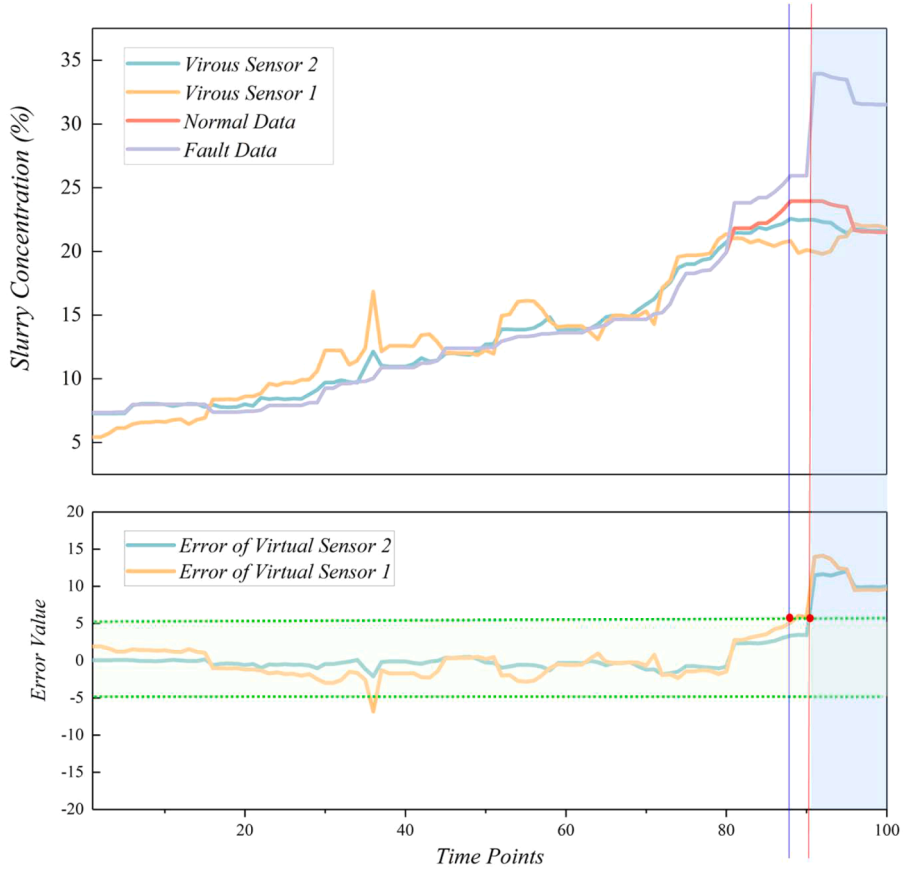

Fig. 11. The performance of HRSFT system in the event of single sensor failure.

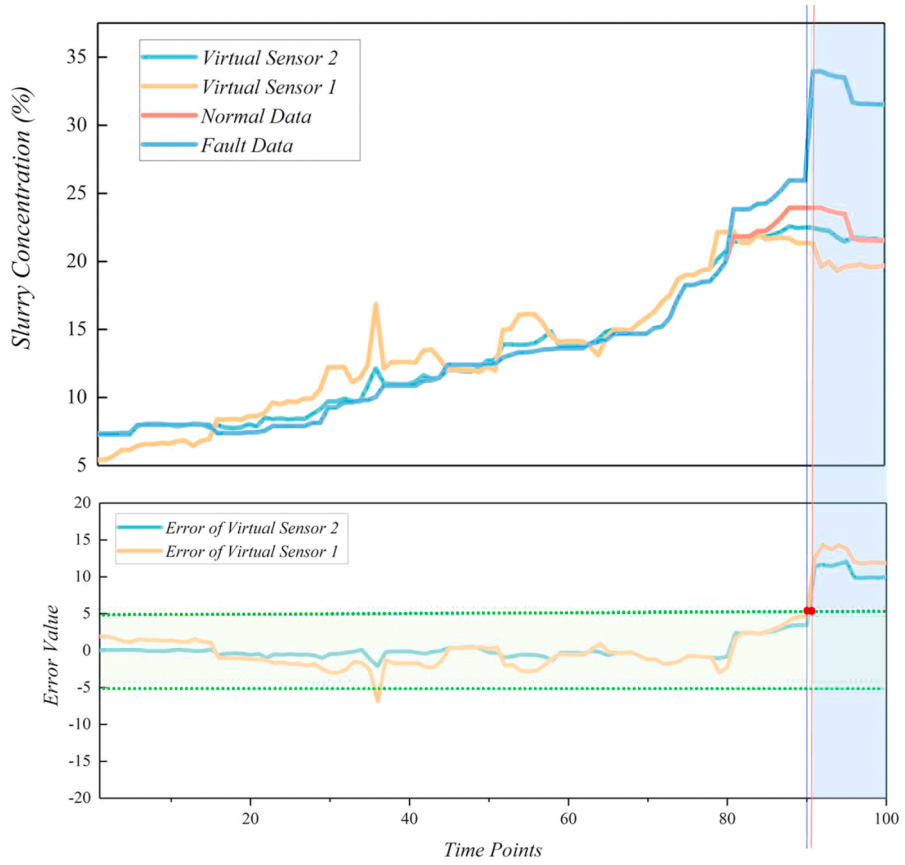

Fig. 12. The performance of HRSFT system in the event of double sensor failure.

6.1. *Detection of single sensor failure*

The two virtual sensor models were built with the training data described above and tested with the test set. The relevant parameters and results of the two models are shown in the Tables 1 and 2.

(Fig. 11)

Fig. 11 illustrates the performance of the two virtual sensors in comparison to the physical sensor. It can be observed that the virtual sensors track the physical sensor more accurately, particularly the performance of VS2 being superior in this regard in this case. During Nos. 30 - 40, when virtual sensor VS1 is in alarm mode and VS2 is not, the system conducts self-tests and continues to output the physical sensor value. Following No. 80, an additive sensor fault occurs, with Nos. 80–90 representing a drift fault of small magnitude. Initially, the HRSFT system fails to detect the alarm upon additive of the drift fault data. As the data magnitude increases, VS1 detects and alarms first, while VS2 does not. In such instances, the system continues to output the value of the physical sensor P. Then, between Nos. 90 and 100, the additive bias fault occurs, with a wider range. Early on in this bias fault, both virtual sensors detect the fault simultaneously. As a result, the HRSFT system triggers a random alarm while outputting a fusion value of VS1 and VS2.

6.2. ***Detection of double sensors failure***

In the case where two and more sensors are detected to be abnormal, the sensor replacement logic is that firstly, the faulty sensor is predicted by the VS2 driven by the time-series model, and then the abnormal sensor information is predicted by the VS1 driven by the multiple regression prediction model based on the normal sensor and VS2 replacement, and finally the data from VS1 and VS2 are fused instead of the abnormal sensor information to complete the replacement. The detection of double sensors failure experiment result as shown in Fig. 12.

The findings presented in Fig. 11 suggest that the system's performance remains relatively consistent prior to point No. 80, which aligns with the behavior observed in the single-sensor-fault experiment. This result demonstrates that the current design is able to effectively address situations involving virtual sensor false alarms, where VS1 detects anomalies during operation, but HRSFT system does not trigger an alarm. Furthermore, the system continues to output physical sensor values under normal circumstances.

However, the data presented after point No. 80 reveals that VS1 identified sensor faults before VS2 did, though not as clearly as in the single-sensor-fault experiment. It is worth noting that in the dual-fault experiment, the alarm value for both virtual sensors is larger than in the single-sensor-fault experiment. These observations suggest that while the system design is able to effectively when presented with dual faults.

6.3. *Detection of multiple sensor failure*

Finally, to verify the response performance of the HRSFT system in the event of multiple sensor malfunction, experiments were conducted where in three sensors were simultaneously rendered inoperative. The experiment results are illustrated in Fig. 13. As with the single-fault and double-fault scenarios, the figures presented in Fig. 13 depict the detection performance achieved and the distance between the residual and threshold.

The combination of Figs. 11–13 reveals that multiple sensor failures can affect the prediction accuracy of the VS1. However, the paper's proposed HRSFT system anomaly disposal method effectively counteracts the impact of simultaneous multiple sensor failures on the performance of VS1. The HRSFT system combines VS1 with VS2 in a stepwise manner, thus enhancing the prediction accuracy even when multiple sensors fail. The effectiveness of the HRSFT system anomaly disposal

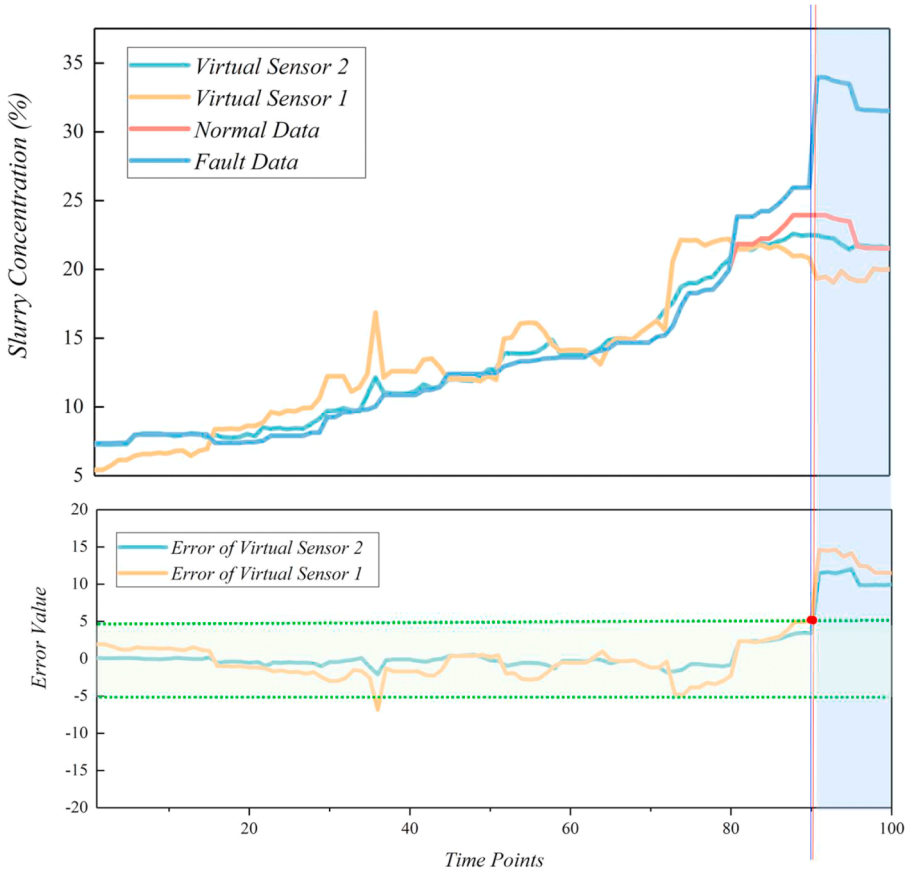

Fig. 13. The performance of HRSFT system in the event of multiple sensor failure.

Table 3
Models comparison.

Models	Normal Stage (No.1 - No.80)	Drift Fault Stage (No.81 – No.90)	Bias Fault Stage (No.91 – No.100)	Total
HRSFT	0	0	0	0
CNN-LSTM	1	1	0	2
CNN	1	2	0	3
Stacking	2	2	0	4

method is supported by the findings in this study.

To further substantiate the superiority of the HRSFT model in comparison with other models, we conducted nine independent iterations of experiments within a multi-sensor failure context. Each iteration involved analyzing a dataset comprising 100 randomly chosen consecutive time series data groups. The results of these experiments, specifically concerning the incidence of false alarms, are presented in the Table 3.

Upon review, it is evident that the HRSFT model achieved a false alarm count of zero. The CNN-LSTM time series model, however, reported one false alarm during the normal stage and another during the drift fault stage, accumulating a total of two false alarms. The CNN-based multivariate regression model registered one false alarm in the normal stage and two in the drift fault stage, totaling three false alarms. The Stacking multivariate regression model noted two false alarms in both the normal and drift fault stage, summing to four false alarms overall. Comparative analyses with other models elucidate the robust anomaly detection capabilities of our HRSFT architecture, underscoring its remarkable reliability.

7. Discussion

In this study, we introduced a voting-cold storage strategy for sensor fault alarm tasks in the context of the DPS. This approach marks a significant advancement over traditional methods, which often rely on single virtual sensors and are prone to false alarms. The incorporation of numerical values and detailed analysis in our results provides a clearer understanding of this strategy's efficacy. Our findings indicate a substantial reduction in false alarms when implementing the voting-cold storage strategy. By integrating virtual and physical sensors effectively, it is possible to significantly enhance measurement accuracy without increasing the number of sensors. The information fusion methodology proposed herein has successfully elevated the precision and lifespan of the sensor system. This innovative approach contributes to the sensory systems of intelligent equipment, facilitating performance optimization across the entire lifecycle of the sensing units. It paves a new pathway for the development of intelligent dredging equipment, offering a novel perspective on the advancement of smart machinery.

On the other hand, the HRSFT method presented in this paper also encounters certain limitations. Its data-driven nature means it is constrained by the quantity and quality of data, leading to insufficient generalizability. The model performs well when applied to the same dredger operating under similar soil conditions. However, its efficacy is not guaranteed when applied to different dredgers or in soil conditions that significantly deviate from the training data. This limitation highlights the need for a more versatile model capable of adapting to varied operational contexts.

In conclusion, the HRSFT strategy represents a notable improvement in sensor system reliability for dredging operations. Its ability to reduce false alarms and provide reliable sensor data is essential for advancing the field of automated dredging. Our study lays the groundwork for

further innovations in this area, with the ultimate goal of enhancing the efficiency, safety, and environmental sustainability of dredging operations.

8. Conclusion

This paper proposed a novel methodology to enhance the reliability of the DPS with Sensor Fault-Tolerant Design. The methodology involved employing two data-driven models, each grounded on distinct principles, to predict sensor information. This data was then utilized to develop a HRSFT system integrated with a physical sensor. This system proved capable of detecting, identifying, isolating, and accommodating sensor anomalies. Compared to a single DB virtual sensor, the HRSFT system's diagnostic accuracy for sensor abnormalities significantly improved. In the module handling faulty sensor information processing and replacement, the values from two virtual sensors were simultaneously fused using weighted least squares and then outputted, particularly when a single sensor fault was detected. In cases of multiple sensor faults, the abnormal information was initially replaced with predictions from VS2, followed by fault sensor data prediction by VS1. Finally, the data from VS1 and VS2 were fused, replacing the abnormal sensor information. Thus, the design substantially increased the precision of the replacement value for the fault sensor.

The data-driven hybrid redundancy sensor configuration presented in this study enhanced system data utilization efficiency and addressed the challenges of high redundancy configuration costs and complex system structures. This approach significantly increased the system's reliability by effectively tackling the issue of simultaneous multiple sensor failures, marking a significant advancement towards practical applications of DB virtual sensors. Future studies will focus on employing transfer learning techniques to enhance the generalization capabilities of our model, aiming to make it more adaptable and effective across diverse operational environments and datasets.

Author statement

On behalf of all co-authors, I, Shidong Fan, hereby declare that the work presented in this manuscript is original research carried out by our collective team. This work has not been published previously, is not currently under consideration for publication elsewhere, in whole or in part. All the research findings reported are novel and have been conducted in a transparent and ethical manner.

No conflict of interest exists in the submission of this manuscript, and the manuscript is approved by all authors for publication. We confirm that each author has contributed significantly to the research and that all listed authors have approved the enclosed manuscript.

The authors would like to acknowledge the financial support from the National Natural Science Foundation of China (Grant No. 52071240), the China Scholarship Council (Grant No. 202206950030), and the 111 Project (Grant No. BP0820028). This funding has been instrumental in the execution of our project.

The order of authors is as follows, reflecting their respective contributions to the work:

We express our collective gratitude to our supporting institutions for their role in facilitating our research.

CRediT authorship contribution statement

Bin Wang: Conceptualization, Methodology, Writing – original draft. **Enrico Zio:** Writing – review & editing, Supervision, Project administration. **Xiuhan Chen:** Writing – review & editing, Formal analysis. **Hanhua Zhu:** Validation, Conceptualization, Investigation, Formal analysis. **Yunhua Guo:** Writing – review & editing, Validation, Software, Formal analysis. **Shidong Fan:** Writing – review & editing, Supervision, Funding acquisition, Project administration, Resources.

Declaration of competing interest

The authors declare that they have no known competing financial interests or personal relationships that could have appeared to influence the work reported in this paper.

Data availability

Data generated or analyzed during the study are available from the corresponding author by request.

Acknowledgements

This work has been supported by National Natural Science Foundation of China (Grant No. 52071240), the China Scholarship Council (Grant No. 202206950030), the State Key Program of National Natural Science Foundation of China (U2341284) and the Programme of Introducing Talents of Discipline to Universities (Grant No. BP0820028). The authors also thank the LASAR (Laboratory of Signal Analysis and Risk Analysis) for helpful discussions and suggestions.

Appendix

A. *Severity (S)*

Severity is the evaluation index of the severity for the impact on product quality and customers when a potential failure mode occurs, which value ranges from 1 to 10.

B. *Occurrence (O)*

Occurrence is the possibility of a potential failure mode, which occurrence rate is between 1 and 10. The scoring criteria are shown in the Table 4.

Table 4
FMEA scale for occurrence.

Probability of Failure	Failure rates	Ranking
Very high: Failure almost inevitable	≥1/2	10
	1/3	9
High: Repeated failures	1/8	8
	1/20	7

(*continued on next page*)

Table 4 (*continued*)

Probability of Failure	Failure rates	Ranking
Moderately: Occasional failures	1/80	6
	1/400	5
Low: Relatively few failures	1/2000	4
	1/15,000	3
Remote: Nearly impossible	1/150,000	2
	≤1/1500,000	1

C. Detection (D)

Detection refers to the evaluation index of the probability that a potential failure can be accurately detected according to the existing methods when a potential failure occurs. Its value ranges from one to ten. The scoring criteria are shown in the Table 5.

Table 5
FMEA scale for detection.

The likelihood of the failure being detected	The probability of not being detected	Ranking
Potential occurring of failure mode cannot be detected in concept, design and process FMEA mechanism and subsequent failure mode.	≥1/2	10
The possibility of detecting the potential occurring of failure mode is very remote/mechanism and subsequent failure mode.	1/3	9
The possibility of detecting the potential occurring of failure mode is remote/mechanism and subsequent failure mode.	1/8	8
The possibility of detecting the potential occurring of failure mode is very low/mechanism and subsequent failure mode.	1/20	7
The possibility of detecting the potential occurring of failure mode is low/mechanism and subsequent failure mode.	1/80	6
The possibility of detecting the potential occurring of failure mode is moderate/mechanism and subsequent failure mode.	1/400	5
The possibility of detecting the potential occurring of failure mode is moderately high/mechanism and subsequent failure mode.	1/2000	4
The possibility of detecting the potential occurring of failure mode is high/mechanism and subsequent failure mode.	1/15,000	3
The possibility of detecting the potential occurring of failure mode is very high/mechanism and subsequent failure mode.	1/150,000	2
The potential occurring of failure mode will be detect/ mechanism and subsequent failure mode.	≤1/1500,000	1

D. Risk Priority Number (RPN)

Risk Priority Number is the product of the Severity, the Occurrence and the Detection, i.e.,$RPN = S \times O \times D$, which value is in Between 1 and 1000. RPN is a comprehensive evaluation index for the occurrence of a potential failure mode and its hazards. Specifically, the item with the highest RPN value should be the focus of preventive control.

After scoring the failure evaluation of eight key parameters by relevant professionals, the results are shown in Tables 6 and 7. More specifically, the severity ranking of all the DPS elements are eight when the sensing system operational reliability in “Fault state”. Similarly, the severity ranking is seven when it is in the “Degradation state”.

Table 6
“Fault states” RPN .

Sensors	S	O	D	RPN
Slurry concentration meter	8	6	1	48
Flow meter	8	5	1	40
Discharge pressure gauge of underwater pump	8	4	1	32
Discharge pressure gauge of main slurry pump	8	4	1	32
Pressure gauge of vacuum degree of underwater pump	8	4	1	32
Cutter rotation measurement	8	3	1	24
Swing speed measurement	8	3	1	24
Cutter power measurement	8	3	1	24

From Tables 6 and 7, we can find that the RPN value of the slurry concentration is the largest in the “fault states” and “degradation state” by the FMEA technology for the DPS. Therefore, we should be focused on preventing its failure. Moreover, in order to simplify the problem, we select the CSD slurry concentration as the research object, analyze the influence of its failure mode, and hence improve the operational reliability of the DPS.

Table 7
“Degradation state” RPN .

Sensors	S	O	D	RPN
Slurry concentration meter	8	9	5	360
Flow meter	8	9	3	192
Discharge pressure gauge of underwater pump	6	3	2	36
Discharge pressure gauge of main slurry pump	6	3	2	36
Pressure gauge of vacuum degree of underwater pump	6	3	2	36
Cutter rotation measurement	6	3	2	26
Swing speed measurement	7	3	2	42
Cutter power measurement	6	3	2	36

References

[1] Wei C, Bai H, Wei Y, Ji Z, Liu Z. Learning manipulation skills with demonstrations for the swing process control of dredgers. Ocean Eng 2022;246:110545.
[2] Wang B, Fan S, Jiang P, Xing T, Fang Z, Wen Q. Research on predicting the productivity of cutter suction dredgers based on data mining with model stacked generalization. Ocean Eng 2020;217:108001.
[3] Wang B, Zio E, Fan S. Reliability evaluation of the hybrid-redundancy sensor fault tolerate system in the dredging perception system. Ocean Eng 2023;281:114844.
[4] Ouyang Z, Liu Y, Ruan SJ, Jiang T. An improved particle swarm optimization algorithm for reliability-redundancy allocation problem with mixed redundancy strategy and heterogeneous components. Reliab Eng Syst Saf 2019;181:62–74.
[5] Cheng D, Lu Z, Zhou J, Liang X. An optimizing maintenance policy for airborne redundant systems operating with faults by using Markov process and NSGA-II. Reliab Eng Syst Saf 2023;236:109257.
[6] Wang S, Yao Y, Ge D, Lin Z, Wu J, Yu J. Reliability evaluation of standby redundant systems based on the survival signatures methods. Reliab Eng Syst Saf 2023;239:109509.
[7] Gao S, Wang J, Zhang J. Reliability analysis of a redundant series system with common cause failures and delayed vacation. Reliab Eng Syst Saf 2023;239:109467.
[8] Amin AA, Hasan KM. A review of fault tolerant control systems: advancements and applications. Measurement 2019;143:58–68.
[9] Zou S, Zhao W, Wang C, Chen F. Fault detection strategy of vehicle wheel angle signal via long short-term memory network and improved sequential probability ratio test. IEEE Sens J 2021;21(15):17290–9.
[10] Niu G, Xiong L, Qin X, Pecht M. Fault detection isolation and diagnosis of multi-axle speed sensors for high-speed trains. Mech Syst Signal Process 2019;131:183–98.
[11] Yang Z, Baraldi P, Zio E. A multi-branch deep neural network model for failure prognostics based on multimodal data. J Manuf Syst 2021;59:42–50.
[12] Peiravi A, Nourelfath M, Zanjani MK. Universal redundancy strategy for system reliability optimization. Reliab Eng Syst Saf 2022;225:108576.
[13] R.V. Beard, "Failure accommodation in linear systems through self-reorganization," Doctoral, Massachusetts Institute of Technology, 1971.
[14] Hassani M, Azimi E, Khodaparast A, Adabi J, Pouresmaeil E. Fault-tolerant operation strategy for reliability improvement of a switched-capacitor multilevel Inverter. IEEE Trans Ind Electron 2022;69(10):9916–26.
[15] Bikdeli E, Adabi J, Rezanejad M, Gholamian SA. Investigation on fault tolerant capability of a single source switched capacitor multilevel inverter. IEEE Trans Ind Electron 2021;68(9):7921–30.
[16] Choi UM, Blaabjerg F, Lee KB. Reliability improvement of a T-type three-level inverter with fault-tolerant control strategy. IEEE Trans Power Electron 2015;30(5):2660–73.
[17] Pinciroli L, Baraldi P, Zio E. Maintenance optimization in industry 4.0. Reliab Eng Syst Saf 2023;234:109204.
[18] Zio E. Prognostics and Health Management (PHM): where are we and where do we (need to) go in theory and practice. Reliab Eng Syst Saf 2022;218.
[19] Wang B, Baraldi P, Zio E. Deep multi-adversarial conditional domain adaptation networks for fault diagnostics of industrial equipment. IEEE Trans Ind Inform 2022;19(8):8841–51.
[20] Gutiérrez León P, García-Morales J, Escobar-Jiménez RF, Gómez-Aguilar JF, López-López G, Torres L. Implementation of a fault tolerant system for the internal combustion engine's MAF sensor. Measurement 2018;122:91–9.
[21] Zhang K, Jiang B, Yan XG, Shen J. Interval sliding mode observer based incipient sensor fault detection with application to a traction device in China railway high-speed. IEEe Trans Veh Technol 2019;68(3):2585–97.
[22] Sun S, Hu W, Liu Y, Wang T, Chu F. Matching contrastive learning: an effective and intelligent method for wind turbine fault diagnosis with imbalanced SCADA data. Expert Syst Appl 2023;223(119891).
[23] Lei Y, Yang B, Jiang X, Jia F, Li N, Nandi AK. Applications of machine learning to machine fault diagnosis: a review and roadmap. Mech Syst Signal Process 2020;138(106587).
[24] Yang Z, Baraldi P, Zio E. A method for fault detection in multi-component systems based on sparse autoencoder-based deep neural networks. Reliab Eng Syst Saf 2022;220:108278.
[25] Cartocci N, Napolitano MR, Costante G, Valigi P, Fravolini ML. Aircraft robust data-driven multiple sensor fault diagnosis based on optimality criteria. Mech Syst Signal Process 2022;170:108668.
[26] Darvishi H, Ciuonzo D, Eide ER, Rossi PS. Sensor-fault detection, isolation and accommodation for digital twins via modular data-driven architecture. IEEE Sens J 2021;21(4):4827–38.
[27] Lin TH, Wang TC, Wu SC. Deep learning schemes for event identification and signal reconstruction in nuclear power plants with sensor faults. Ann Nucl Energy 2021;154.
[28] Luo XJ, Fong KF, Sun YJ, Leung MKH. Development of clustering-based sensor fault detection and diagnosis strategy for chilled water system. Energy Build 2019;186:17–36.
[29] Gautam S, Tamboli PK, Patankar VH, Roy K, Duttagupta SP. Sensors incipient fault detection and isolation using kalman filter and Kullback–Leibler divergence. IEEE Trans Nucl Sci 2019;66(5):782–94.
[30] Amin AA, Iqbal MS, Shahbaz MH. Development of intelligent fault-tolerant control systems with machine learning, deep learning, and transfer learning algorithms: a review. Expert Syst Appl 2024;238:121956.
[31] Wang B, et al. A novel method with stacking learning of data-driven soft sensors for mud concentration in a cutter suction dredger. Sensors 2020;20(21):6075 (Basel).
[32] Wang B, et al. The replacement of dysfunctional sensors based on the digital twin method during the cutter suction dredger construction process. Measurement 2022;189:110523.
[33] Li M, Lu Q, Bai S, Zhang M, Tian H, Qin L. Digital twin-driven virtual sensor approach for safe construction operations of trailing suction hopper dredger. Autom Constr 2021;132:103961.
[34] Haji-Esmaeili MM, Naseri M, Khoun-Jahan H, Abapour M. Fault-tolerant structure for cascaded H-bridge multilevel inverter and reliability evaluation. IET Power Electron 2017;10(1):59–70.
[35] Zhang W, Xu D, Enjeti PN, Li H, Hawke JT, Krishnamoorthy HS. Survey on fault-tolerant techniques for power electronic converters. IEEE Trans Power Electron 2014;29(12):6319–31.
[36] Wang B, Fan S, Jiang P, Chen Y, Zhu H, Xiong T. Cutting state estimation and time series prediction using deep learning for Cutter Suction Dredger. Appl Ocean Res 2023;134:103515.
[37] Zou S, Zhao W, Liang W, Wang C, Chen F. Fault diagnosis and fault-tolerant compensation strategy for wheel angle sensor of steer-by-wire vehicle via extended Kalman filter. IEEE Sens J 2022;22(2):1756–66.
[38] Liu HC, Wang LE, Li Z, Hu YP. Improving risk evaluation in FMEA with cloud model and hierarchical TOPSIS method. IEEE Trans Fuzzy Syst 2019;27(1):84–95.
[39] Alanen J, et al. Hybrid ontology for safety, security, and dependability risk assessments and Security Threat Analysis (STA) method for industrial control systems. Reliab Eng Syst Saf 2022;220:108270.